

MODELLING AND EXPERIMENTAL STUDY OF A PASSIVE FREQUENCY-DEPENDENT VEHICLE SUSPENSION DAMPER

Bartłomiej FRANCZYK*, JANUSZ GOŁDASZ**

*Faculty of Mechanical Engineering, Cracow University of Technology, al. Jana Pawła II 37, 31-864 Kraków, Poland
 **Faculty of Electrical and Computer Engineering, Cracow University of Technology, ul. Warszawska 24, 31-155 Kraków, Poland

bartlomiej.franczyk@doktorant.pk.edu.pl, jgoldasz@pk.edu.pl

received 28 Septemeber 2023, revised 24 November, accepted 7 January 2024

Abstract: The recent trends in the automotive industry have enforced chassis solutions beyond the reach of conventional systems. Thus, extending the functionality of passive hydraulic dampers is vital in improving their effectiveness while maintaining low production and operating costs. This paper presents a general structure of a passive shock absorber with so-called frequency-dependent (FD) damping characteristics and points to constitutive elements of the valves used in this type of an adaptive damper. A mathematical description of FD damper is provided together with a model developed in the Siemens AMESim environment. The performance of the model was verified against the data from tests with a real, commercially available FD shock absorber. Furthermore, in order to emphasise its efficiency, the authors have carried out a study involving quarter car models (QCM) with and without the FD damper, respectively. The results have clearly shown major advantages of utilising FD dampers in a suspension.

Key words: vehicle dynamics, ride, road holding, adaptive damping, quarter car, frequency dependent damping

1. INTRODUCTION

In general, motor vehicles are subjected to constant vibrations of a random nature, the source of which are road irregularities and driving manoeuvres. Vehicle dampers that are used in suspensions systems are aimed at providing sufficient amount of damping, and thus satisfying level of driving comfort as well as good handling and roadholding of a vehicle. However, it is known that these criteria are most often contradictory, and the level of damping in the suspension is the result of a compromise between smooth ride and adequate motion control [1, 2]. The reason for this conflict can be well understood by analysing exemplary transmissibility function of a classic one degree of freedom (1-DOF) harmonic oscillator. As one can see in Fig. 1, an increase in damping coefficient reduces or even eliminates the resonant peak corresponding to the sprung mass natural frequency. On the other hand, higher damping degrades isolation from road inputs at the higher frequency excitations. Thus, high damping is required in the suspension system for frequencies below the invariant point of $\omega_0\sqrt{2}$, while above this frequency low damping would be most beneficial [3]. This conflict is amplified by the fact that the vehicle suspension consists of sprung mass and several unsprung masses, which differ by an order of magnitude. Due to such a significant difference, each of these masses needs different damping forces to be tuned optimally. Wheel vibrations, usually of high frequency but small amplitude, require less damping forces than vibrations of a vehicle body, which are characterised by low frequency and high amplitude [4, 5]. It becomes obvious that for the overall improvement of vehicle dynamics, damping dependent on current operating conditions of the suspension should be used with particular emphasis on operation frequencies.

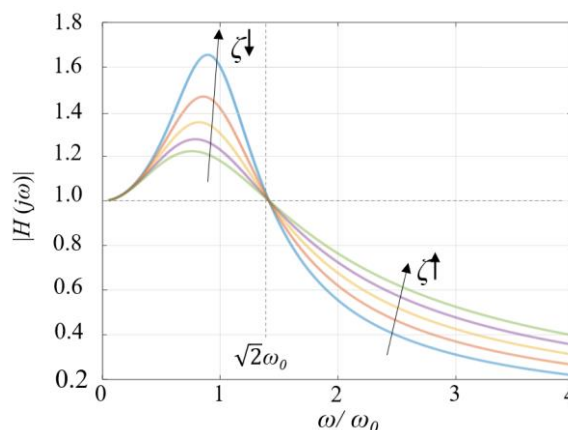


Fig. 1. Displacement transmissibility function of a 1-DOF harmonic oscillator: $H(j\omega)$ – the ratio of input and output amplitudes, ω – excitation frequency, ω_0 – natural frequency, ζ – damping coefficient. 1-DOF, one degree of freedom

One common way of making the damper operation dependent on the excitation frequency (or the excitation change rate in general) is the use of active or semi-active systems utilising electronic controls. Some benefits of such systems have been described in the works of Nguyen et al. [6], Slaski [7] and Pletschen et al. [8]. However, such solutions are relatively expensive and thus unavailable to ordinary car owners. Obviously, far more affordable technologies would rely on passive valving systems configured for the desired functionality. This category includes both displacement-sensitive dampers (DSD) and amplitude-sensitive dampers (ASD) [9, 10]. Notable DSD examples include, for instance, the works of Lee and Moon [11], Hazaveh et al. [12] and Ilbeigi et al. [13]. Such dampers allow for the position dependency of the

damping force in order to increase ride comfort at low amplitude inputs while keeping sufficient body control at high amplitude inputs. It should be noted, however, that such valving systems operate well only when the damper's relative displacement amplitude oscillates around their design positions where the DSD feature are usually located. If the initial position of the suspension changes significantly as in the case of a loaded vehicle, it may exhibit unexpected and disadvantageous behaviours. This shortcoming seems to be avoided when ASD valving systems are used. With these systems, the damping level depends on the amplitude of the suspension movement, regardless of the initial position; low damping is provided for low-amplitude inputs but whenever damper travel exceeds a certain amount, damping increases significantly. The ASD examples are described by Łuczko and Ferdek [14], Łuczko et al. [15], Goldasz [16] and Zhang et al. [9]. ASD systems, however, are not free of disadvantages, namely, a sudden change in the level of forces related to the full use of the working range of elastic elements involved, increased noise or a large number of additional components [9]. Moreover, due to the time delay needed to reach high damping forces, they can negatively affect the vehicle's steering system response. Some authors, for example, Nie et al. [17] carried out attempts to achieve even more sophisticated damper characteristics and thus bringing the passive damper's performance closer to that of the active one. Xu et al. [18] presented a damper with a variable moment of inertia to improve vehicle chassis dynamic characteristics. Finally, Sikora [19] proposed a tuned mass damper in order to achieve improved dynamic characteristics with no apparent negative impact on the steady-state performance. It must be noted, however, that real implementations of such concepts usually require difficult-to-realise technological solutions.

Based on the above considerations, it can be concluded that the optimal solution to achieve both high levels of comfort (or isolation from road inputs) and driving performance is a suspension damper possessing variable damping characteristics, independent of the suspension position, providing reduced damping forces at high-frequency and low-amplitude inputs, but at the same time delivering 'normal' levels of damping forces at low frequency and high amplitude excitations. These requirements seem to be met by frequency-dependent (FD) dampers [20, 21]. With these dampers, they behave as typical, passive dampers at low frequencies and gradually decrease the magnitude of their output at the higher ones. An in-depth review of available and patented solutions in this area was carried out by Franczyk et al. [10]. The authors have shown that most FD-like valves on the market have been developed as add-on system in parallel to the main valves usually operating in the rebound portion of the damper's working cycle. In rare cases, the FD valve is integrated into base (foot) valve assemblies of twin-tube dampers [21].

It is acknowledged by the authors that the term 'frequency-dependent valve' may be misleading; the reader should refer to Dixon [22] for further discussion on the topic. In the essence, FD type valves are pressure-rate dependent valves. In the presented study, the authors simply follow the nomenclature used by automotive OEMS and other parties involved in the development of the FD technology in passenger vehicles.

To summarise, the purpose of this work is to provide a complete, functional math model of the FD damper, which can become the basis for further component level parametric studies. The authors claim that their proposed valve architecture is sufficient to copy the operating principles of most FD damping sys-

tems. The model is verified experimentally to ensure that it is capable of reproducing the characteristics of a real FD shock absorber. To the best knowledge of the authors, no such model of the valve has been presented so far and so it is novel. The second goal is to examine the impact of the FD damper on the comfort and safety of a car.

2. MATERIALS AND METHODS

This subsection presents both the method of modelling the FD shock absorber as well as the performance of a quarter model of a car equipped with this type of shock absorber.

2.1. Passive twin-tube FD damper

In this paragraph a model of a twin-tube, passive adaptive vehicle damper is presented and developed. The damper's structure is shown simply in Fig. 2. As shown, the piston and rod assembly (A) divides the inner volume into the compression chamber (B) and the rebound chamber (C). The reserve chamber (D) is formed by the volume between the inner and the outer tubes. The base valve (E) further separates the oil volume in the reservoir from the compression chamber. The volume of the rebound (upper) chamber is V_r and the pressure in the chamber is p_r . Similarly, the volume of the compression chamber (below the piston) is V_c and the compression pressure is referred to as p_c . Moreover, the gas pressure is p_g , and the volume V_g . While in compression, the oil flows from the compression chamber to the rebound chamber and, in a volume equal to the volume of the piston rod being forced into the damper, to the reserve chamber. In the rebound (upward) stroke the flows are reversed. The references volumetric flow rates are marked in Fig. 2 by means of the following abbreviations: Q_{PVC} – flow rate between the chambers (B) and (C) through the compression side shim stack of the piston valve, Q_{PVR} – flow rate between the chambers (C) and (B) through the rebound side shim stack of the piston valve, Q_{PVO} – flow rate through the constant area orifice in the piston valve assembly linking directly the chambers (B) and (C), Q_{BVC} – flow rate between the chambers (B) and (D) through the compression side shim stack of the base valve assembly, Q_{BVR} – flow rate between the chambers (D) and (B) through the rebound side shim stack of the base valve assembly, Q_{BVO} – flow rate through the constant area orifice located in the base valve. The model assumes the presence of the FD valve assembled within the piston valve and arranged to operate specifically in the damper's rebound stroke, in parallel to the main rebound valve (Q_{FD}). The FD valve, in general, utilises the basic operation principle of conventional damper valves which means it can be considered as a shim or blow-off valve whose opening depends on the pressure difference across it. The main difference, however, is that it is additionally controlled by pilot pressure, which causes its hardening or softening depending on the pressure rate in the main rebound chamber of the shock absorber. The presented solution corresponds to most commercial architectures of the FD valves and incorporates the following three characteristic elements: the accumulator chamber of variable volume, the constant area control orifice (CO) located at its inlet and a pressure-controlled relief valve operated as a by-pass in parallel to the main rebound valve [10]. The hydraulic scheme of the described piston valve assembly is shown in Fig. 3.

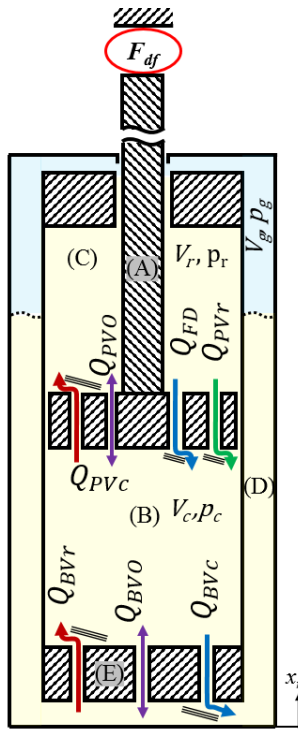


Fig. 2. Diagram of the analysed FD damper

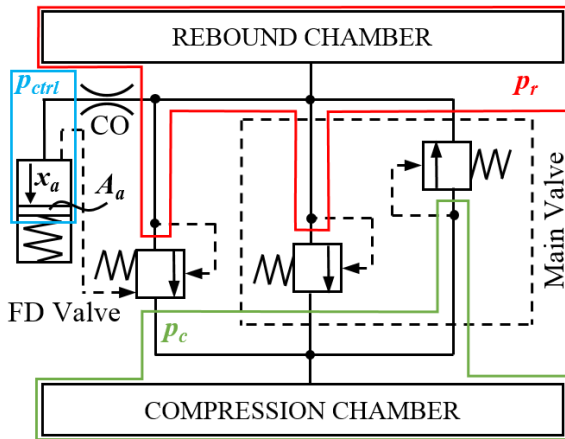


Fig. 3. Hydraulic circuit of the piston valve assembly

To start with, taking into account the compressibility of the oil, both rebound and compression pressures (\$p_r, p_c\$) can be calculated using the following expressions [23]:

$$\begin{cases} \dot{p}_r = \beta \frac{(A_p - A_{pr})\dot{x}_r - Q_{PV}}{V_r} \\ \dot{p}_c = \beta \frac{-A_p\dot{x}_r + Q_{PV} + Q_{BV}}{V_c} \\ V_r = V_{r0} + (A_p - A_{pr})x_r \\ V_c = V_{c0} - A_p x_r \end{cases} \quad (1-4)$$

where \$\beta\$ refers to the oil bulk modulus, \$A_p\$ and \$A_{pr}\$ are the cross-section areas of the piston and piston rod, respectively, \$V_r\$ and \$V_c\$ are the volumes and \$V_{r0}\$ and \$V_{c0}\$ are the initial volumes of the rebound and compression chambers, respectively, \$x_r\$ is the displacement of the damper body with respect to the piston rod and \$Q_{PV}\$ and \$Q_{BV}\$ denote the total oil flow rates through the piston valve and the base valve. Based on the diagram in Fig. 1, the respective flow rates are defined as:

$$Q_{PV} = \begin{cases} Q_{PVO} + Q_{PVR} + Q_{FD} & \text{if } p_r - p_c > 0 \\ 0 & \text{if } p_r - p_c = 0 \\ Q_{PVO} + Q_{PVC} & \text{if } p_r - p_c < 0 \end{cases} \quad (5)$$

$$Q_{BV} = \begin{cases} Q_{BVO} + Q_{BVR} & \text{if } p_c - p_g > 0 \\ 0 & \text{if } p_c - p_g = 0 \\ Q_{BVO} + Q_{BVC} & \text{if } p_c - p_g < 0 \end{cases} \quad (6)$$

where \$p_g\$ is the gas pressure.

The oil flow rates through the two orifice flow rates \$Q_{PVO}\$ and \$Q_{BVO}\$ are modelled by means of the modified Bernoulli equation as follows [23, 24]:

$$Q = c_o A \sqrt{\frac{2\Delta p}{\rho}} \quad (7)$$

where \$Q\$ is the respective flow rate, \$c_o\$ refers to the dynamic discharge coefficient; piston valve – \$c_{PVO}\$, base valve – \$c_{BVO}\$. The pressure difference \$\Delta p\$ is calculated as \$\Delta p = p_r - p_c\$ (piston valve) or \$\Delta p = p_c - p_g\$ (base valve), and \$\rho\$ is the oil density.

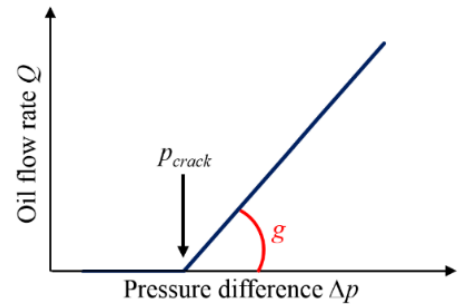


Fig. 4. Generic flow characteristic of the pressure-relief valve

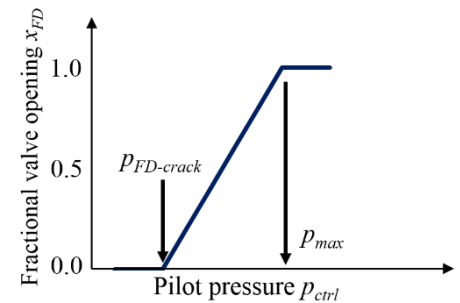


Fig. 5. Opening characteristic of the pilot-operated pressure-relief valve

For the sake of clarity of the presented analysis, it is assumed that at high damper velocities the flows are realised by means of hydraulic pressure-relief valves, best characterised by the nonlinear relationship \$Q(\Delta p)\$. Modelling the behaviour of shim valves is, therefore, outside the scope of this study. That has been well described, for example, by Skačkauska et al. [24], Xu et al. [25], Czop et al. [26] and Farjoud and Ahmadian [27]. In this study the authors further employ a more simplified functional approach. In this manner oil flow rates through each of the four relief-valves can be described using the following relationships [28]:

$$Q_{PVR} = \begin{cases} 0 & \text{if } p_r - p_c \leq p_{PVR-crack} \\ g_{PVR}(p_r - p_c) |p_r - p_c| & \text{if } p_r - p_c > p_{PVR-crack} \end{cases} \quad (8)$$

$$Q_{PVC} = \begin{cases} 0 & \text{if } p_c - p_r \leq p_{PVC-crack} \\ g_{PVC}(p_c - p_r)|p_c - p_r| & \text{if } p_c - p_r > p_{PVC-crack} \end{cases} \quad (9)$$

$$Q_{BVR} = \begin{cases} 0 & \text{if } p_g - p_c \leq p_{BVR-crack} \\ g_{BVR}(p_g - p_c)|p_g - p_c| & \text{if } p_g - p_c > p_{BVR-crack} \end{cases} \quad (10)$$

$$Q_{BVC} = \begin{cases} 0 & \text{if } p_c - p_g \leq p_{BVC-crack} \\ g_{BVC}(p_c - p_g)|p_c - p_g| & \text{if } p_c - p_g > p_{BVC-crack} \end{cases} \quad (11)$$

where g_{PVR} , g_{PVC} , g_{BVR} , and g_{BVC} are constant coefficients for defining slopes of the $Q(\Delta p)$ curve as shown in Fig. 4. The pressures $p_{PVR-crack}$, $p_{PVC-crack}$, $p_{BVR-crack}$, and $p_{BVC-crack}$ are cracking pressures of the pressure-relief valves in the piston assembly and the base valve one. Based on this approach, the flow through each valve is initiated only upon exceeding the specific cracking pressure.

As shown in Fig. 3, the FD portion of the rebound valve assembly includes a more complex valve which is modelled here with a pilot-operated pressure-relief valve. The opening of the valve x_{FD} is governed by the pilot (control) pressure p_{ctrl} , the pressure due to the spring pre-tension $p_{FD-crack}$ and the pilot differential pressure p_{max} at maximum opening as revealed in Fig. 5. Then, the flow rate through the FD valve can be simply described as follows [17]:

$$Q_{FD} = \begin{cases} 0 & \text{if } x_{FD} = 0 \\ C_{FD} A_{FD} x_{FD} \sqrt{\frac{2(p_r - p_c)}{\rho}} & \text{if } 0 < x_{FD} < 1 \\ C_{FD} A_{FDmax} \sqrt{\frac{2(p_r - p_c)}{\rho}} & \text{if } x_{FD} = 1 \end{cases} \quad (12)$$

where C_{FD} is the dynamic discharge coefficient of the FD valve, A_{FDmax} is the maximum valve cross-sectional area and $A_{FD} = x_{FD} A_{FDmax}$ is the valve cross-sectional area due to its fractional (dimensionless) valve opening x_{FD} computed as:

$$x_{FD} = \frac{p_{ctrl} + p_{crack} - p_r}{p_{max}} \quad (13)$$

The pilot pressure p_{ctrl} is calculated considering the dynamics of the accumulator chamber and the CO. Assuming that $p_{ctrl} > F_{0a}/A_a$, where A_a is the accumulator's cross-sectional area and F_{0a} denotes the preload force in the accumulator (due to the spring preload or a precharge pressure), the flow rate into the accumulator's chamber Q_a is:

$$Q_a = A_a \dot{x}_a \quad (14)$$

where x_a is the displacement of the spring-loaded piston in the accumulator. By balancing the forces acting on the piston the following equation is obtained:

$$p_{ctrl} A_a = k_a x_a \quad (15)$$

where k_a is the stiffness ratio of the accumulator's spring. By differentiating Eq. (15), the following equation is obtained

$$p_{ctrl} \dot{A}_a = k_a \dot{x}_a \quad (16)$$

and combining Eqs (14) and (16) yields:

$$p_{ctrl} \dot{A}_a = Q_a \frac{k_a}{A_a^2} \quad (17)$$

It must be noted that the flow rate Q_a is equal to the flow rate through the orifice CO located at the inlet into the accumulator chamber. Applying Eq. (7) here, one obtains:

$$Q_a = c_{CO} A_{CO} \sqrt{\frac{2(p_r - p_{ctrl})}{\rho}} \quad (18)$$

and finally:

$$p_{ctrl} \dot{A}_a = \frac{k_a}{A_a^2} c_{CO} A_{CO} \sqrt{\frac{2(p_r - p_{ctrl})}{\rho}} \quad (19)$$

The variation of the gas pressure p_g can be obtained by using the adiabatic relationship [24]:

$$p_g = p_{g0} \left(\frac{V_{g0}}{V_g} \right)^n = p_{g0} \left(\frac{V_{g0}}{V_{g0} + \int_0^t Q_{BV} dt} \right)^n \quad (20)$$

where p_{g0} is the initial gas pressure, V_g is the gas volume, V_{g0} is the initial gas volume and n is an adiabatic index.

Finally, the force output F_{df} can be expressed considering the pressures acting on the piston:

$$F_{df} = (A_p - A_{pr}) p_r - A_p p_c + p_g A_{pr} \quad (21)$$

Given the set of Eqs (1)–(21), a mathematical model is developed in Siemens AMESim environment ver. 2022 – see Fig. 6. The model parameters were altered to fit the characteristics of a commercially available FD type damper for which experimental data were extracted using the test rig revealed in Section 2.3. The adopted model parameters are listed in Tab. 1.

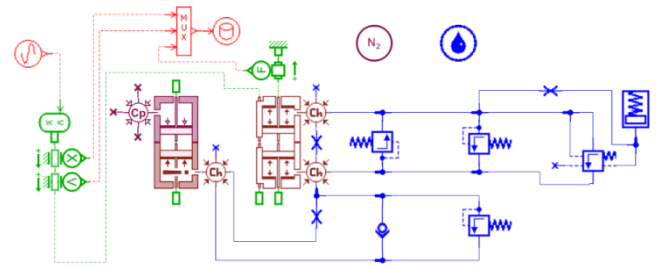


Fig. 6. Structure of the AMESim simulation model of the analysed FD damper

Tab. 1. Set of AMESIM model parameters

Damper and oil parameters								
A_p [mm ²]	A_{pr} [mm ²]	p_{g0} [MPa]	V_{g0} [m ³]	n [–]	β [Pa]	ρ [kg/m ³]	V_{r0} [dm ³]	V_{c0} [dm ³]
1017.4	254.3	0.6	0.02	1.4	17,000	850	0.06	0.08
Piston valve parameters								
A_{PVO} [mm ²]	C_{PVO} [–]	g_{PVR} [m ³ /s/MPa]	g_{PVC} [m ³ /s/MPa]	$p_{PVR-crack}$ [MPa]	$p_{PVC-crack}$ [MPa]			
2.2	0.99	$3.8 \cdot 10^{-4}$	$1.3 \cdot 10^{-3}$	1.52	0.12			

Base valve parameters								
A_{BVO} [mm ²]	c_{BVO} [·]	g_{BVR} [m ³ /s/MPa]	g_{BVC} [m ³ /s/MPa]	$\rho_{BVR-crack}$ [MPa]	$\rho_{BVC-crack}$ [MPa]			
0.5	0.93	$1.7 \cdot 10^{-3}$	$2.7 \cdot 10^{-4}$	0.0	1.0			
FD valve parameters								
A_{CO} [mm ³]	F_{0a} [N]	A_a [mm ²]	k_a [N/mm]	c_{CO} [·]	c_{FD} [·]	A_{FDmax} [mm ²]	$\rho_{FD-crack}$ [MPa]	ρ_{max} [MPa]
0.16	150	397	950	0.7	0.7	5.6	0.7	0.25

2.2. 2-DOF quarter car model

A classic two degree of freedom (2-DOF) quarter car model (QCM) is used in order to study the effectiveness of using FD dampers in passenger vehicles. Such model is a common tool suitable for ride comfort and vehicle safety evaluation studies, respectively [5, 6, 11, 29]. As it is shown in Fig. 7, it consists of the sprung (body) and unsprung (wheel) masses connected by spring and damping elements. There is a spring element placed between the unsprung mass and the ground (road input) which represents the elasticity of a tire. The QCM equations of motion are then as follows:

$$M_w \ddot{z}_2 = k_t(z_2 - x_0) - k_s(z_1 - z_2) - c_s(\dot{z}_1 - \dot{z}_2) \quad (22)$$

$$M_b \ddot{z}_1 = k_s(z_1 - z_2) - c_s(\dot{z}_1 - \dot{z}_2) \quad (23)$$

where M_w is the mass of the wheel (kg), M_b refers to the mass of the vehicle body (kg), k_t is the tire stiffness ratio (N/m), k_s is the suspension spring stiffness ratio (N/m), c_s denotes the damping coefficient (Ns/m), z_1 and z_2 are the displacements of the vehicle body and wheel, respectively, and x_0 is the road input.

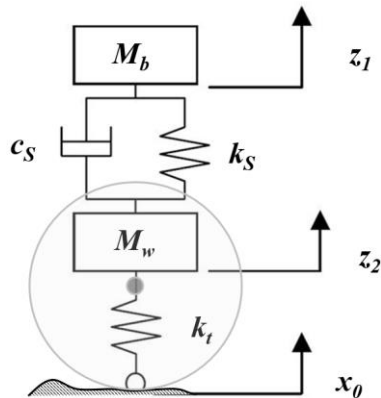


Fig. 7. A 2-DOF QCM

In this paper, two QCMs of the parameters presented in Tab. 2 are studied in terms of ride comfort and safety. The values of M_w , M_b , k_t , and k_s are adopted to suit a front quarter of a vehicle of total weight of 2,400 kg distributed between front and rear axles with the ratio of 60:40 and having the body natural frequency of 0.7 Hz. In this first scenario the authors study the performance of a QCM with a standard damper, whereas the second scenario involves the FD damper with the low frequency performance identical to the standard damper and FD valve parameters as presented in Tab. 1. The QCM models are presented in Fig. 8.

As highlighted in Fig. 9, the reduction in the output forces is ≈ 400 N at the frequency of 12 Hz, which in relative terms results in 40% degradation achieved at the velocity of $v = 0.15$ m/s and 17% at the velocity of $v = 1.0$ m/s.

Tab. 2. QCM parameters

M_w [kg]	M_b [kg]	k_t [kN/m]	k_s [kN/m]
30	720	200	15

QCM, quarter car model.

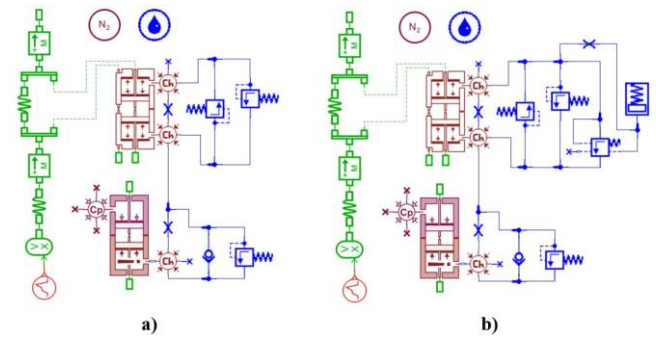


Fig. 8. QC model with (a) a conventional damper, (b) a FD damper

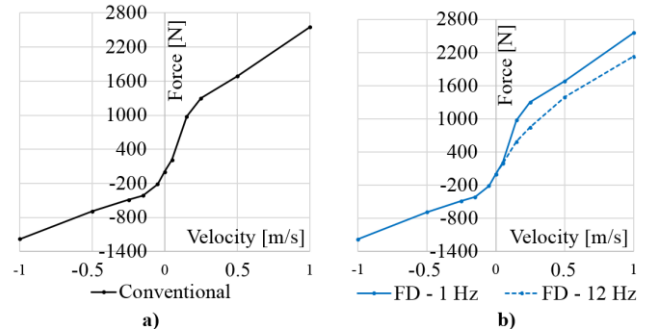


Fig. 9. Measured performance characteristics of (a) a conventional (non-FD) damper, (b) a FD damper

The QCMs were excited with stochastic ISO 8086 type road displacement signals. The ISO 8086 standard provides means for classifying road surface types depending on their quality (roughness) and describes various approaches to be used in order to simulate specific road surface profiles. In this paper, artificial road profiles of the ISO classes A–B (very good), C–D (average) and E–F (very poor), as shown in Fig. 10, are generated using the method similar to the one used in Agostinacchio et al. [30]. For each of the generated road profiles the following three cases are studied varying in the vehicle horizontal velocity – 36 km/h, 72 km/h and 108 km/h (10 m/s, 20 m/s and 30 m/s, respectively). In each case the driving distance is equal to 300 m. Testing the dynamic properties of a vehicle by means of QCM and ISO standardised profiles is an effective and proven method [14, 29, 30]. The selected range of road profiles and driving speeds takes into account the range of operating conditions to which passenger cars are commonly subjected [29, 30].

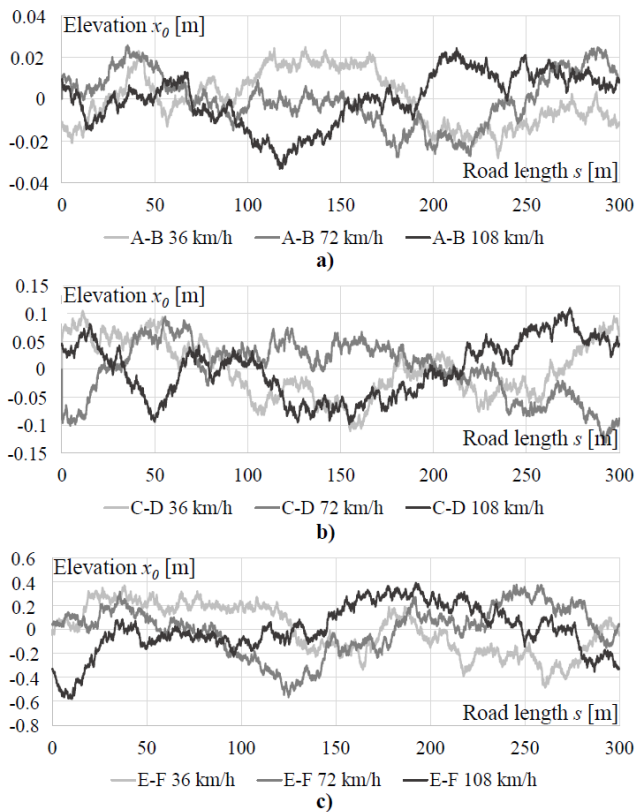


Fig. 10. Generated road profiles for three distinct vehicle's velocities, (a) A-B, (b) C-D and (c) D-E

2.3. Damper test setup, inputs

The damping force measurements of a commercially available passive FD twin-tube damper were measured using the hydraulic test rig shown in Fig. 11.

The MTS stoker was equipped with a MTS 661.21A-01 force transducer with a capacity of 25 kN and a MTS Silentflo 505.11 hydraulic pump capable of flow rates up to 41.5 l/min and the

output pressures up to 207 bar. The damper was mounted in the rig as shown in the photograph with the bottom rigidly attached to the moving base, whereas the piston rod was held stationary. All signals (displacement, velocity, force) were acquired simultaneously at the sampling rate of 1 kHz. The prescribed input displacement was a sinewave resulting in peak velocities up to 0.5 m/s and the frequencies up to 15 Hz. Such testing is the industry standard for most shock absorbers, although specific test speeds depend on manufacturer requirements and suspension design. The test frequencies were selected to cover the range of resonant frequencies of sprung masses and unsprung masses of a typical passenger car, which are usually within the range from ≈ 1.3 Hz to 15 Hz, respectively [1]. The experiment plan of both the laboratory experiments and the numerical simulations covered 75 subsequent test runs according to Tab. 3.

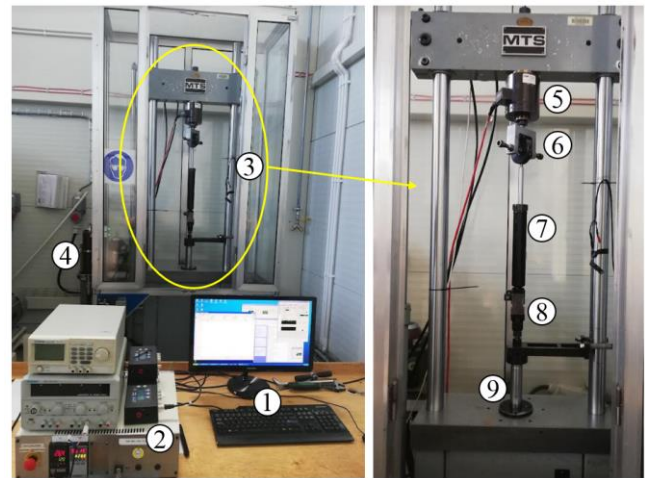


Fig. 11. Test rig for damper performance measurements; 1 – PC with dedicated software for data acquisition, 2 – control unit, 3 – stoker frame, 4 – hydraulic power supply, 5 – force transducer, 6 – upper mount, 7 – test sample, 8 – lower mount, 9 – stoker rod (exciter).

Tab. 3. Test plan for both simulations and rig tests; the input displacement amplitude a (mm) varies with the peak velocity v and the frequency f

f [Hz] v [m/s]	1	2	3	4	5	6	7	8	9	10	11	12	13	14	15
0.05	8.0	4.0	2.7	2.0	1.6	1.3	1.1	1.0	0.9	0.8	0.7	0.7	0.6	0.6	0.5
0.15	23.9	11.9	8.0	6.0	4.8	4.0	3.4	3.0	2.7	2.4	2.2	2.0	1.8	1.7	1.6
0.25	39.8	19.9	13.3	9.9	8.0	6.6	5.7	5.0	4.4	4.0	3.6	3.3	3.1	2.8	2.7
0.35	55.7	27.9	18.6	13.9	11.1	9.3	8.0	7.0	6.2	5.6	5.1	4.6	4.3	4.0	3.7
0.50	79.6	39.8	26.5	19.9	15.9	13.3	11.4	9.9	8.8	8.0	7.2	6.6	6.1	5.7	5.3

3. RESULTS AND DISCUSSION

In this section the authors reveal the results of two modelling studies. First, the mathematical model of the FD damper is verified experimentally. Second, the QCM based analysis is carried out to access the influence of the FD-damper on comfort and safety metrics.

3.1. FD damper model verification

The accuracy of the model is verified by comparing the damping forces from obtained during the experiments and those in the simulations. The comparison is carried out in the form of static force-velocity plots as well as force-velocity and force-displacement diagrams, respectively. This is a popular method of evaluating damper models in the literature [11, 24, 25].

The obtained results are presented in Figs 12–14. In more detail, Figs 12 and 13 illustrate the output of the model in the form of force–velocity and force–displacement plots, respectively, at three various excitation frequencies $f = \{1, 6, 12\}$ Hz and the two peak

velocities $v = \{0.25, 0.50\}$ m/s. Finally, Fig. 14 shows the static force-velocity and force-frequency curves at various frequencies and velocities.

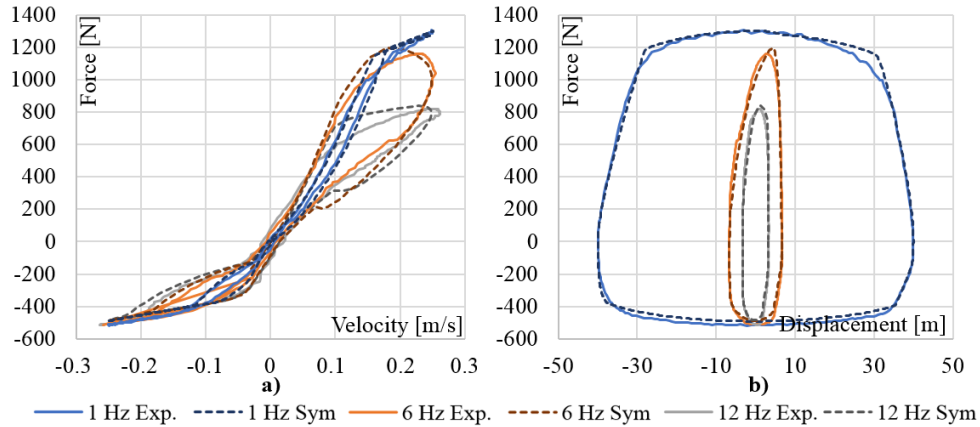


Fig. 12. Model vs experiment, $v = 0.25$ m/s – (a) force vs velocity, (b) force vs displacement

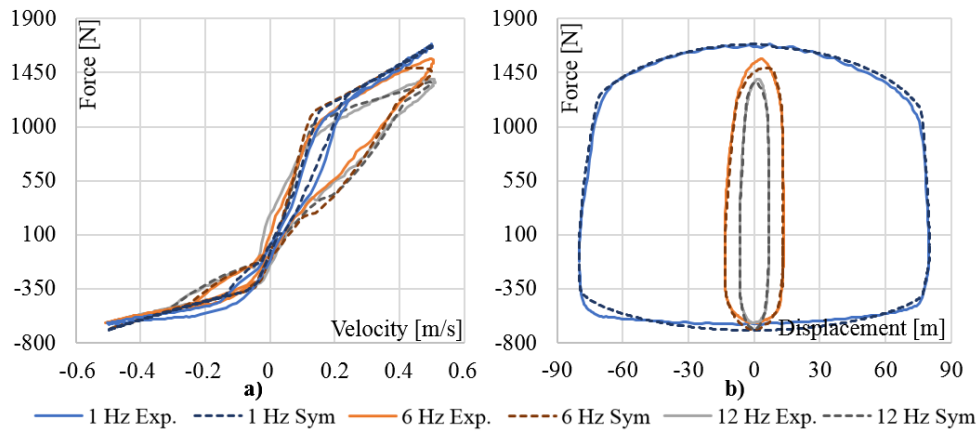


Fig. 13. Model vs experiment, $v = 0.50$ m/s – (a) force vs velocity, (b) force vs displacement

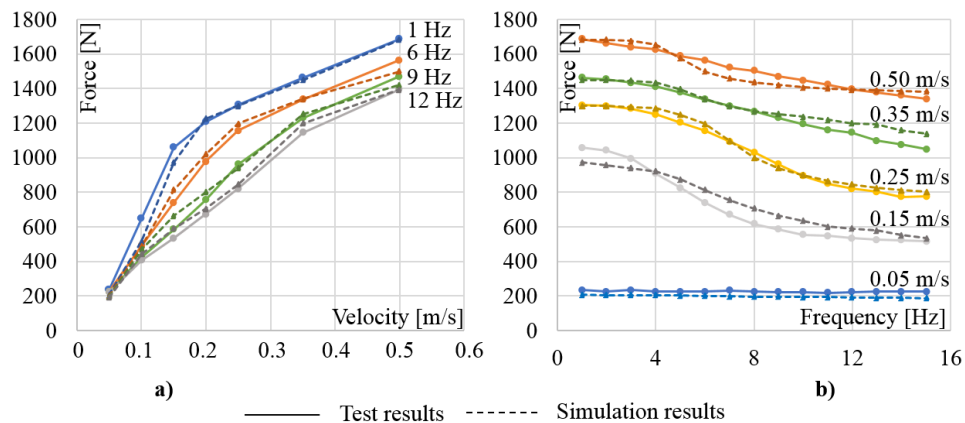


Fig. 14. Model vs experiment; variation of the damping force with frequency and velocity (a) force vs velocity plot, (b) force falloff (force vs frequency) diagram

In order to assess the model’s accuracy in predicting the output of the analysed FD damper, relative error metrics were calculated according to the equation below:

$$\delta = \frac{|F_{exp} - F_{sym}|}{F_{exp}} \cdot 100\% \quad (24)$$

where F_{exp} and F_{sym} are damping force values obtained from experimental and simulation tests, respectively. The results are presented in Tab. 4. As shown, the mismatch varies from 0% to nearly 17%. It should be noted, however, that the largest error value is obtained at low damper velocities, where the forces are

small (~200 N). The average error value over the entire frequency range for the velocities from 0.15 m/s to 0.50 m/s is 4%.

Our analysis of the obtained data shows that at the smallest input velocity of 0.05 m/s the force variation against the frequency is almost negligible. However, as the frequency of the input increases the output forces degrade gradually by ~400 N. Considering the contents of Tab. 4, the best agreement at the velocities is obtained at the input velocities >0.05 m/s. It is also evident from the data that the model maintains the typical performance of a passive damper at the lowest frequency. This effect is the most distinctive feature of the FD technology, which sets them apart from the rest of the adaptive dampers. Due to this feature, FD

damper application in a suspension may ensure good support for the vehicle body at low frequencies. On the other hand, at high frequencies, the damping force is built up much more slowly over time, so that the energy of small but frequent vibrations is not transferred to the body, which in turn ensures better comfort. The above comparison of the simulation results and the experimental measurements indicates a good match between the output of the real damper and its mathematical model. Thus, it can be concluded that the presented model accurately reflects the functionality of the FD type adaptive damper and can be successfully used in further research.

Tab. 4. Relative error metrics δ (%): model vs experiment

f [Hz] v [m]	1	2	3	4	5	6	7	8	9	10	11	12	13	14	15	Avg
0.05	11	9	12	9	11	12	15	13	12	13	12	13	15	17	17	13
0.15	8	8	6	1	6	10	12	14	13	14	10	10	10	5	4	9
0.20	2	2	4	4	6	4	6	6	6	6	6	5	4	4	4	5
0.25	0	0	1	3	4	3	1	3	2	1	2	3	3	5	3	2
0.35	1	0	1	1	1	0	0	0	2	4	5	5	9	8	9	3
0.50	0	1	2	2	1	4	4	5	3	3	2	0	1	2	3	2
Avg	3	3	4	3	4	5	6	6	6	6	5	5	6	6	6	x

3.2. Analysis of QCM output

The definition of vehicle ride comfort refers to the unpleasant feelings experienced by vehicle passengers and caused by vibrations. It is often evaluated by means of the weighted root-mean-square (RMS) acceleration of the sprung mass according to the following equation [29, 31, 32]:

$$RMS(\ddot{z}_1) = \sqrt{\frac{\int_0^T \ddot{z}_1^2(t) dt}{T}} \quad (25)$$

where T is the simulation time. In order to compare damping effectiveness of FD damper in relation to a conventional one in terms of ride comfort, a reduction factor is calculated as follows:

$$\delta_{RMS(\ddot{z}_1)} = \left(1 - \frac{RMS(\ddot{z}_{1-FD})}{RMS(\ddot{z}_{1-C})}\right) \times 100\% \quad (26)$$

where $RMS(\ddot{z}_{1-FD})$ and $RMS(\ddot{z}_{1-C})$ refer to the calculated RMS values involving FD and conventional damper scenarios, respectively.

Next, vehicle's road holding ability directly depends on the tire's ability to stay in contact with the road and to transfer both longitudinal and lateral forces. One commonly used indicator of this performance is the value of the tire normal force T_i , which influences the friction between the tire and the road surface. In this context, the aim is to obtain the highest possible force with a stable course. On the other hand, too much force, especially when dynamic overloads occur, can damage the suspension components. In this paper, road holding indicators are calculated and compared in a manner similar to the ride comfort metric presented above. For this purpose, the variable \ddot{z}_1 is replaced by F_i in the Eqs (25) and (26) and so the following road-holding metrics are obtained:

$$RMS(F_t) = \sqrt{\frac{\int_0^T F_t^2(t) dt}{T}} \quad (27)$$

$$\delta_{RMS(F_t)} = \left(1 - \frac{RMS(F_{t-FD})}{RMS(F_{t-C})}\right) \times 100\% \quad (28)$$

It should be noted that more elaborate evaluation methods exist for both ride comfort and road-holding metrics for passenger vehicles [30, 33–35]. However, for the purpose of this study, which is a preliminary research preceding more elaborated ones, the authors have decided to use the fundamental metrics.

Fig. 15 highlights exemplary sections of the acceleration \ddot{z}_1 and the force F_i in time domain, obtained for the ISO C–D road profile and the vehicle's horizontal velocity of 72 km/h. Fig. 16 presents a summary of the examined RMS metrics.

On analysing the results, it becomes evident that an FD damper's QCM is most effective when driven on middle-class quality roads. Note, however, that the study is limited to one specific FD damper tuning only. In the examined case up to 12% reduction in $RMS(\ddot{z}_1)$ can be observed with the average impact of 2.7% on road holding performance. When driven on good quality roads, the comfort level is increased up to 7% with a negligibly small impact on safety. The biggest yet still small impact of the FD damper on tire loads can be observed when driven on poor quality road of the E–F ISO class. It should be noted, however, that at high driving speeds, this effect is highly beneficial, as it protects the tire from overloading, as in this case the dynamic tire loads reach up to 150% of the tire static load. In particular, examining the contents of Fig. 15, it can be easily observed that the time history of acceleration is much smoother in the case of the FD-based QCM. As seen, most of the sharp peaks are removed, which may be beneficial not only for the passenger's comfort but also for improvement in noise/harshness; acceleration peaks are reduced by up to 40% (see Fig. 15 at $t = 3.02$ s).

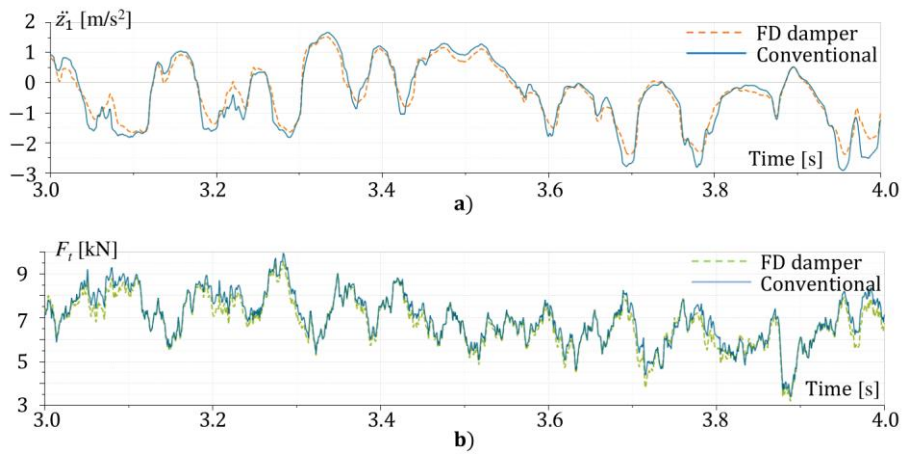


Fig. 15. Time history of (a) body vertical acceleration \ddot{z}_1 and (b) tire normal force F_t : conventional damper vs FD damper; profile – ISO C–D at 72 km/h

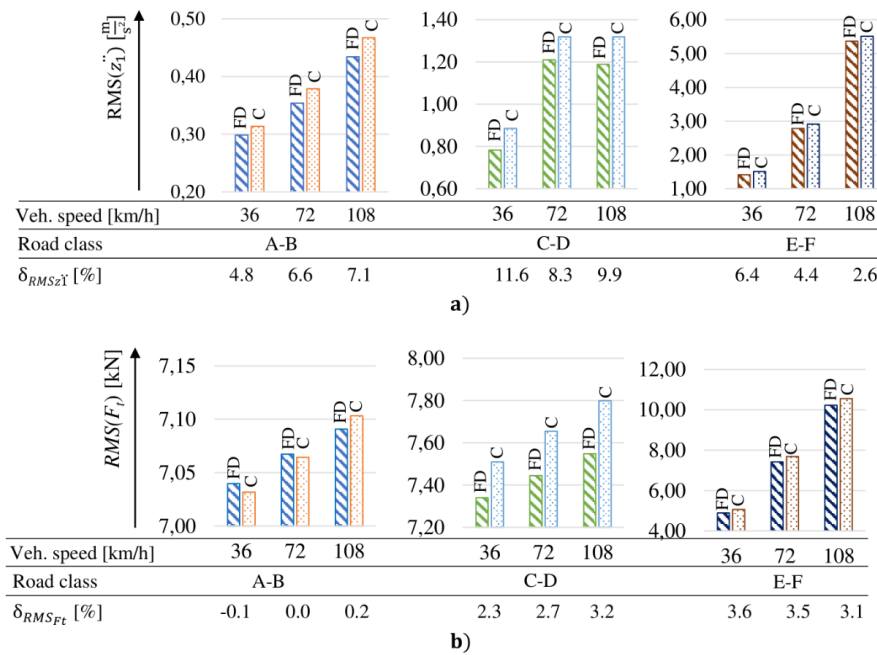


Fig. 16. RMS and δ_{RMS} metrics: (a) vehicle body acceleration \ddot{z}_1 , (b) tire normal force F_t

4. CONCLUSIONS

The purpose of the present study was to provide a dynamic, experimentally verified, functional model of a twin-tube FD damper and to examine its impact on vehicle ride comfort and safety. To the best knowledge of the authors, the hydraulic circuit of the presented model of the FD damper corresponds to the existing solutions available on the automotive market; the model assumes the presence of the FD valve housed within the piston valve assembly and operating on the rebound side of the piston valve in parallel to the main valve assembly. The developed model was verified experimentally across a wide range of frequencies and velocity inputs. It copies the essential features of FD type valving systems, that is, reduction of pressures with the increase of the excitation input frequency. The model is of functional character and presents the principle of operation on which the FD damper technologies are based. It is not design nor configuration oriented.

Furthermore, the simulation studies conducted by means of simple QCM models indicate that the use of the FD damper in vehicles results in improved driving comfort levels with a negligible impact on road holding performance. Depending on the type of

surface and driving conditions, the improvement in comfort levels is up to 12%, while the impact on safety does not exceed 4%. In all examined cases, the trade-off between comfort and safety favours the use of FD dampers. The improvements in comfort metrics are supported not only by the obtained RMS values of the body acceleration, but also by the fact that their peak values are smoothed and significantly reduced. Therefore, further improvement in terms of noise and harshness are likely. It must be noted, however, that the research presented in this paper covers one specific case of a vehicle and damper and so broader research must be conducted in order to generalise the conclusions.

The presented model is novel. To our knowledge, no math models of FD type suspension dampers capable of copying the damping force variation with the frequency of the excitation have been developed so far. The FD technology has been present on the automotive market for the last 20 years (mostly as aftermarket solutions) and it has gained the approval of the OEMs recently as the industry tends to seek new solutions in on-going efforts to meet the customer expectations in terms of comfort, handling and NVH using passive damping technologies. The FD dampers may fill in the gap between the conventional passive suspension sys-

tems and more sophisticated state-of-the-art electronically controlled real-time ones. The technology is simple yet effective and easy to integrate into the existing passive valve assemblies. As such, a model that is capable of copying the dynamic behaviour of such valves may be a valuable asset in the vehicle development work.

Finally, the authors plan to develop a parametric model of the FD valve linked to the geometry of a specific FD valve concept so that the model can be an aid in the valve development and engineering process.

REFERENCES

- Neal MW, Cwycyshyn W, Badiru I. Tuning Dampers for Ride and Handling of Production Vehicles. *SAE International*. 2015;8(1):152–9.
- Badiru I, Cwycyshyn WB. Customer focus in ride development. *SAE International*. 2013;2013(1):1355.
- Rajmani R. *Vehicle Dynamics and Control*, 2nd ed. Springer New York Dordrecht Heidelberg London. 2012.
- Sekulić D, Dedović V. The Effect of Stiffness and Damping of the Suspension System Elements on the Optimisation of the Vibrational Behaviour of a Bus. *International Journal for Traffic and Transport Engineering*. 2011;1:231–44.
- Solmaz S, Afatsun AC, Başlamışlı SÇ. Parametric analysis and compensation of ride comfort for electric drivetrains utilizing in-wheel electric motors. *International Journal of Simulation: Systems, Science and Technology*. 2016;17(33).
- Nguyen LH, Hong KS, Park S. Road-frequency adaptive control for semi-active suspension systems. *Int J Control Autom Syst*. 2010;8(5):1029–38.
- Slaski G. Simulation and experimental testing of adaptive suspension damping control depending on the frequency of a sinusoidal kinematic input. *The Archives of Automotive Engineering*. 2014;2(64):165–78.
- Pletschen N, Spirk S, Lohmann B. Frequency-selective adaptive control of a hybrid suspension system. *IFAC Proceedings Volumes*. 2013;46(21):237–42.
- Zhang Y, Guo K, Li SE, Shao X, Zheng M. Prototyping design and experimental validation of membranous dual-cavity based amplitude selective damper. *Mech Syst Signal Process*. 2016;76–77:810–22.
- Franczyk B, Maniowski M, Goldasz J. Frequency-dependent automotive suspension damping systems: State of the art review. *Proceedings of the Institution of Mechanical Engineers, Part D: Journal of Automobile Engineering [Internet]*. 2023;0(0). Available from: <https://doi.org/10.1177/09544070231174280>
- Lee CT, Moon BY. Simulation and experimental validation of vehicle dynamic characteristics for displacement-sensitive shock absorber using fluid-flow modelling. *Mech Syst Signal Process*. 2006;20(2):373–88.
- Hazaveh NK, Rodgers GW, Chase JG, Pampanin S. Experimental Test and Validation of a Direction- and Displacement-Dependent Viscous Damper. *J Eng Mech*. 2017;143(11).
- Ilbeigi S, Jahanpour J, Farshidianfar A. A novel scheme for nonlinear displacement-dependent dampers. *Nonlinear Dyn*. 2012;70(1):421–34.
- Łuczko J, Ferdek U. Nonlinear dynamics of a vehicle with a displacement-sensitive mono-tube shock absorber. *Nonlinear Dyn*. 2020 Mar 1;100(1):185–202.
- Łuczko J, Ferdek U, Łatas W. Nonlinear analysis of shock absorbers with amplitude-dependent damping. *AIP Conf Proc*. 2018;1922(1):100011.
- Goldasz J. Modelling of amplitude-selective-damping valves. *Mechanics and Control*. 2011;30(2):60–4.
- Nie S, Zhuang Y, Wang Y, Guo K. Velocity & displacement-dependent damper: A novel passive shock absorber inspired by the semi-active control. *Mech Syst Signal Process*. 2018 Jan 15;99:730–46.
- Xu T, Liang M, Li C, Yang S. Design and analysis of a shock absorber with variable moment of inertia for passive vehicle suspensions. *J Sound Vib*. 2015 Oct 27;355:66–85.
- Sikora M. Modeling and Operational Analysis of an Automotive Shock Absorber with a Tuned Mass Damper. *Acta Mechanica et Automatica*. 2018;12(3).
- De Kock P, De Rooter AAW. Shock absorber with frequency-dependent damping. WO 03/040586 A1 (Patent), 2003.
- Nowaczyk M, Van de Plas J, Vochten J. Shock Absorber With Frequency Dependent Passive Valve. United States; US9638280B2, 2017.
- Dixon JC. *The Shock Absorber Handbook*. 2nd ed.. John Wiley & Sons, Ltd; 2007.
- Sikora M. Study of Flow-Induced Vibration Phenomena in Automotive Shock Absorbers. *Mechanics and Control*. 2014;33(2).
- Skačkauskas P, Žuraulis V, Vadluga V, Nagurnas S. Development and verification of a shock absorber and its shim valve model based on the force method principles. *Eksplotacija i Niezawodność - Maintenance and Reliability*. 2017;19(1):126–33.
- Xu J, Chu J, Ma H. Hybrid modeling and verification of disk-stacked shock absorber valve. *Advances in Mechanical Engineering*. 2018;10(2).
- Czop P, Ślawik D, Śliwa P, Wszolek G. Simplified and advanced models of a valve system used in shock absorbers Analysis and modelling. *Journal of Achievements in Materials and Manufacturing Engineering*. 2009;33(2).
- Farjoud A, Ahmadian M. Shim stack deflection analysis in hydraulic dampers using energy methods. In: *Active and Passive Smart Structures and Integrated Systems 2010*. 2010.
- Siemens Industry Software NV. *Simcenter Amesim*. Siemens; 2018.
- Mahmood M, Nassar A, Mohammad H. Analysis and Study Indicators for Quarter Car Model with Two Air Suspension System. *Basrah journal for engineering science*. 2022;22(2).
- Agostinacchio M, Ciampa D, Olita S. The vibrations induced by surface irregularities in road pavements - a Matlab® approach. *European Transport Research Review*. 2014;6(3).
- Wang P. Effect of electric battery mass distribution on electric vehicle movement safety. In: *Vibroengineering Procedia*. 2020.
- Huang S, Nguyen V. Influence of dynamic parameters of electric-vehicles on the ride comfort under different operation conditions. *Journal of Mechanical Engineering, Automation and Control Systems*. 2021;2(1).
- Sharma SK, Kumar A. Ride comfort of a higher speed rail vehicle using a magnetorheological suspension system. *Proceedings of the Institution of Mechanical Engineers, Part K: Journal of Multi-body Dynamics*. 2018;232(1):32–48.
- Deubel C, Ernst S, Prokop G. Objective evaluation methods of vehicle ride comfort — A literature review. *Journal of Sound and Vibration*. 2023; 548:117515.
- Burkhard G, Berger T, Enders E, Schramm D. An extended model of the ISO-2631 standard to objectify the ride comfort in autonomous driving. *Work*. 2021; 68(s1):37–45.

This work was supported by the Ministry of Education and Science of the Republic of Poland under Grant DWD/5/0240/2021.

Bartłomiej Franczyk:  <https://orcid.org/0000-0002-7566-996X>

Janusz Goldasz:  <https://orcid.org/0000-0002-0226-3360>



This work is licensed under the Creative Commons BY-NC-ND 4.0 license.